PHOTONICS Research

Multiple-quantum-well-induced unipolar carrier transport multiplication in AlGaN solar-blind ultraviolet photodiode

Long Guo,[1,2] Ke Jiang,[1,2,4] Xiaojuan Sun,[1,2] Zihui Zhang,[1,3] Jianwei Ben,[1,2] Yuping Jia,[1,2] Yong Wang,[1,2] and Dabing Li[1,2,5]

[1]State Key Laboratory of Luminescence and Applications, Changchun Institute of Optics, Fine Mechanics and Physics, Chinese Academy of Sciences, Changchun 130033, China
[2]Center of Materials Science and Optoelectronics Engineering, University of Chinese Academy of Sciences, Beijing 100049, China
[3]Key Laboratory of Electronic Materials and Devices of Tianjin, School of Electronics and Information Engineering, Hebei University of Technology, Tianjin 300401, China
[4]e-mail: jiangke@ciomp.ac.cn
[5]e-mail: lidb@ciomp.ac.cn

Received 5 July 2021; revised 25 July 2021; accepted 27 July 2021; posted 29 July 2021 (Doc. ID 435937); published 8 September 2021

AlGaN solar-blind ultraviolet (SBUV) detectors have potential application in fire monitoring, corona discharge monitoring, or biological imaging. With the promotion of application requirements, there is an urgent demand for developing a high-performance vertical detector that can work at low bias or even zero bias. In this work, we have introduced a photoconductive gain mechanism into a vertical AlGaN SBUV detector and successfully realized it in a *p-i-n* photodiode via inserting a multiple-quantum-well (MQW) into the depletion region. The MQW plays the role of trapping holes and increasing carrier lifetime due to its strong hole confinement effect and quantum confinement Stark effect. Hence, the electrons can go through the detector multiple times, inducing unipolar carrier transport multiplication. Experimentally, an AlGaN SBUV detector with a zero-bias peak responsivity of about 0.425 A/W at 233 nm is achieved, corresponding to an external quantum efficiency of 226%, indicating the existence of internal current gain. When compared with the device without MQW structure, the gain is estimated to be about 10^3 in magnitude. The investigation provides an alternative and effective approach to obtain high current gain in vertical AlGaN SBUV detectors at zero bias.

https://doi.org/10.1364/PRJ.435937

1. INTRODUCTION

Ultraviolet light in the solar-blind band (200–280 nm) hardly radiates to the Earth's surface due to the strong atmospheric absorption. Therefore, solar-blind ultraviolet (SBUV) detectors have attracted tremendous interest in the scope of fire monitoring, high-voltage equipment corona discharge monitoring, or biological imaging [1–5]. AlGaN material, with a tunable wide bandgap and high absorption coefficient from 3.4 to 6.2 eV, is one of the most suitable materials for SBUV detectors [6]. Moreover, AlGaN SBUV detectors have the advantage of small-size, low-power-consumption, and easy-integration over the most frequently used photomultiplier tubes that feature high vacuum, high voltage, and huge volume [7–9]. Although considerable progress has been made on AlGaN SBUV detectors in recent years, the performance still cannot meet the requirements of real applications because of the poor crystal quality and *p*-doping efficiency deterioration with increasing Al content [10,11]. In order to obtain optimal device performance on the platform with the current AlGaN material quality and *p*-doping efficiency, the structures have been extensively studied and finely optimized.

AlGaN-based detectors generally exhibit five structures, including photoconductor [12], photovoltaic metal-semiconductor-metal (MSM) [13], Schottky diode [14], *p-n* (*p-i-n*, *p-i-n-i-n* or *p-i-p-i-n*) diode [15–17], bipolar transistor, and tripolar transistor [18,19]. The photoconductor can have high gain due to the carrier trapping effect of the surface or internal defects, but the persistent photoconductivity phenomenon that can sustain several tens of seconds or even longer strongly limits its application [20,21]. The photovoltaic MSM structure can avoid the *p*-doping of AlGaN, while it usually has low responsivity and slow response speed due to the symmetrical back-to-back Schottky barriers and long carrier drift length, respectively [22,23]. Besides, the photoconductor and photovoltaic MSM structure generally cannot respond under zero bias, which means that an external power supply is required, leading to extra noise and energy consumption. Although the application of asymmetric electrodes provides zero-bias response through

the asymmetric Schottky barriers, the external quantum efficiency (EQE) is too low [24,25]. Furthermore, the horizontal distributed electrodes make it difficult to fabricate high-pixel focal plane arrays, also limiting their application. Similarly, the tripolar transistor also possesses these disadvantages despite of its high current gain [26,27]. For a long time, researchers have pinned their hopes on the vertical high-gain avalanche photodiodes; however, the premature breakdown, high work voltage, and complex driving circuit crucially restrict their application [8,28,29].

Therefore, there is an urgent need to exploit vertical high-gain structures for AlGaN SBUV detectors, especially at zero bias. However, traditional vertical structures such as the Schottky diode, *p-n* diode, and bipolar transistor generally have no current gain at zero bias. The reported highest EQE and the corresponding responsivity of AlGaN SBUV Schottky diode at zero bias, to our best knowledge, are 53% and 0.115 A/W at 270 nm [30], respectively. There is no current gain in the device, obviously. As for the AlGaN SBUV *p-n* diode, by adopting techniques, including the intrinsic absorption layer, high-quality AlN template, and polarization-graded *p*-AlGaN layer, EQE and responsivity as high as 92% and 0.211 A/W at 289 nm are reached at zero bias [15]. However, the current gain is also not obtained. In terms of the AlGaN SBUV bipolar transistor, most of the reports focus on the visible-blind ultraviolet band [18,31–33], and the only SBUV detector reported shows a low EQE and responsivity of just 1.2% and 0.003 A/W at 280 nm [34], which may result from the low *p*-doping efficiency of Al-rich AlGaN. Consequently, alternative gain mechanism needs to be introduced to vertical structures to realize high EQE and responsivity in AlGaN SBUV detectors.

In this work, we have proposed a strategy of introducing a photoconductive gain mechanism into the vertical AlGaN SBUV detector and have realized it in a *p-i-n* photodiode through inserting the multiple-quantum-well (MQW) into the depletion region. The MQW can generate current gain due to its strong hole confinement effect and the quantum confinement Stark effect (QCSE), inducing long carrier lifetime and unipolar carrier transport, which are the key factors for photoconductive gain. Experimentally, an AlGaN SBUV detector with zero-bias responsivity of 0.425 A/W at 233 nm is achieved, corresponding to an EQE of about 226%, which indicates a significant internal current gain. Compared with the structure without MQW, the gain is estimated to be about 10^3 in magnitude. The MQW can also reduce the dark current because of the large band offset in the MQW, indicating a better signal-to-noise ratio (SNR). This investigation paves the way for fabricating high-gain AlGaN SBUV detectors with vertical structures at low or even zero bias.

2. DEVICE PRINCIPLE

As noted, there are two gain mechanisms in the AlGaN SBUV detector, i.e., photoconductive and avalanche gains. As for the avalanche gain, it is necessary to reach the critical electric field, which is high for Al-rich AlGaN materials. This leads to a high work voltage and complex quenching circuit. However, as for the photoconductive gain, the high voltage and complex circuit are not essential. In order to effectively introduce photoconductive gain in vertical structures, it is required to clearly understand the key factors for determining the gain.

The photoconductive gain can be calculated through Eq. (1):

$$G = \tau \cdot (1/t_{rn} + 1/t_{rp}), \tag{1}$$

where G is the photoconductive gain, τ is the carrier lifetime, and t_{rn} and t_{rp} are the electron and hole transit times, respectively. Here, the electron and hole transit times t_{rn} and t_{rp} are determined by Eq. (2):

$$t_{rn} = L/\mu_n E, \qquad t_{rp} = L/\mu_p E, \tag{2}$$

where L is the drift length, E is the internal electric field, and μ_n and μ_p represent the electron and hole mobility, respectively. In a vertical photovoltaic detector, the drift length is generally short and the built-in electric field is strong in the carrier drift region. Accordingly, the photoconductive gain can be improved by prolonging the carrier lifetime in a vertical photovoltaic detector. Besides, there is another gain mechanism in the photoconduction mode. If one type of carrier drifts much faster than the other and the transit time of the faster carriers is shorter than the lifetime, the carriers will travel through the electrodes several times to keep electrical neutrality, leading to unipolar carrier transport multiplication. Therefore, trapping one type of carrier in the transport region can also increase the photoconductive gain.

Based on the previous analyses, structures that can prolong the carrier lifetime and trap one type of carriers shall be designed into the vertical AlGaN SBUV detectors. Wurtzite AlGaN materials possess strong spontaneous and piezoelectronic polarizations, which can induce a strong built-in electric field in their MQW structures. Figure 1(a) shows an AlGaN single quantum well along the [0001] direction. As can be seen, the built-in electric field in the well layer is along the [000–1] direction, while that in the barrier layer is opposite. The carriers with opposite charge polarities in the well layer can be separated by the built-in electric field and then concentrate at different regions, which is known as the QCSE. The QCSE causes the wave function overlap of electrons and holes to decrease, resulting in the suppressed recombination probability. Correspondingly, the carrier lifetime can be obviously prolonged by utilizing MQW, resulting in photoconductive gain. On the other hand, because the effective mass of holes is much higher than that of electrons, and because the intervalley scattering of electrons is much less than that of holes [8], the holes are easier to be confined by the quantum wells than electrons. As a result, the unipolar carrier transport will be achieved and the photoconductive gain will be increased. Consequently, it is believed that the photoconductive gain can be generated in a vertical AlGaN SBUV *p-i-n* photodiode by inserting MQW into their intrinsic depletion region.

Figure 1(b) illustrates our basic device structure design. An MQW structure is introduced into the depletion region of a vertical back-illuminated *p-i-n* photodiode. To induce photoconductive gain, the MQW has to be inserted between the *i*-layer and *p*-layer. Upon illumination, the photogenerated electron-hole pairs will be mainly produced in the *i*-layer and then swept to the opposite directions by the built-in electric field. The electrons with high mobility are quickly swept

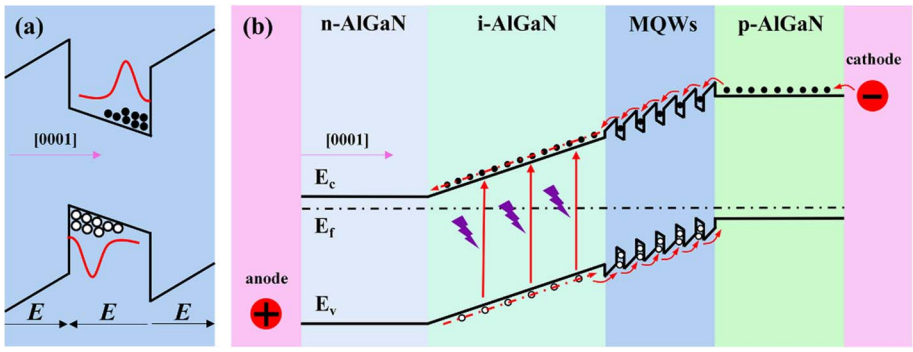

Fig. 1. (a) QCSE in a single quantum well. (b) Energy band diagram of AlGaN SBUV *p-i-n* photodiode with MQW in the intrinsic depletion region.

out to the *n*-layer and extracted by the anode. Meanwhile, the holes will pass through the MQW region. The MQW will reduce the hole mobility due to the scattering effect and trap the hole due to its quantum confinement effect. Furthermore, the recombination rate is diminished by the MQW because of the QCSE, resulting in longer carrier lifetime. In this case, abundant holes will remain in the depletion region. To maintain electrical neutrality, electrons will again drift into the depletion region. Because the mobility of electrons is inherently much higher than that of holes and the intervalley scattering of electrons is less frequent than that of holes, the electrons can traverse the detector multiple times during the lifetime to generate current gain. Further, the MQW can also reduce the dark current of the device and thus enhance the SNR.

3. MATERIALS AND METHODS

A. Simulations

Numerical simulations are conducted by APSYS to verify the effects of the MQW on the carrier transport properties in the AlGaN SBUV *p-i-n* photodiode. Figure 2(a) exhibits the AlGaN SBUV *p-i-n* photodiode structure with MQW in the depletion region, labeled as device S_A. For comparison, the device with the same structure except for the MQW, which is replaced by *i*-AlGaN, is constructed, as shown in Fig. 2(b), labeled as device S_B. In the simulations, the barrier of the MQW is AlN of 8 nm and the well is $Al_{0.20}Ga_{0.80}N$ of 2 nm. The barrier and well alternately repeat for 10 times, and the MQW ends with an AlN barrier, resulting in a total thickness of 108 nm and an average optical-Al-content of 50%. For the reference device S_B, to ensure the same carrier drift length and optical absorption, the thickness and Al content of the *i*-AlGaN layer are set as 108 nm and 50%, respectively. The carrier transport properties are simulated by self-consistently solving the Schrodinger equation, Poisson equation, continuity equation, and drift-diffusion equation with proper boundary conditions. The hole and electron mobilities are set as 5 and 1000 $cm^2/(V \cdot s)$ [35,36], respectively. The conduction and valance band offset ratio for AlGaN heterojunctions and MQW is set as 50/50, leading to both conduction and valance band offsets of 1.1 eV in the MQWs [37]. The polarization level is set to 30%. The optical absorption coefficients for AlGaN layers are extracted from Refs. [38,39].

B. Materials Growth

The devices are grown on single-polished *c*-sapphire substrates by a high temperature metal organic chemical vapor deposition system. The trimethyl aluminum (TMAl), trimethyl gallium (TMGa), and ammonia (NH_3) are used as Al, Ga, and N precursors, respectively. The hydrogen (H_2) is used as the carrier gas. Besides, the silicane (SiH_4) and bis-cyclopentadienyl magnesium (Cp_2Mg) are used as the *n*- and *p*-type doping sources, respectively. First, an AlN template of about 2 μm is grown on the sapphire substrate at 1300°C to improve the quality of upper-device function layers. Then, the temperature is decreased to 1180°C and the transition layers as well as a 500 nm undoped $Al_{0.60}Ga_{0.40}N$ buffer layer are grown on the AlN template to release the stress. Next, the designed device

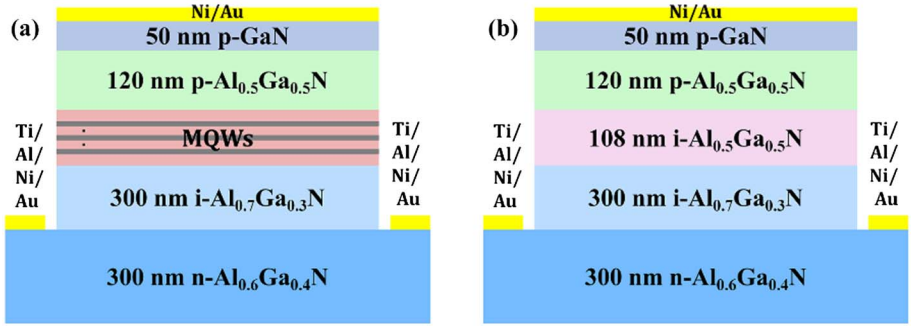

Fig. 2. Photodiode structures (a) with and (b) without MQW.

structures as shown in Fig. 2 are grown. For device S_A, a 300 nm *n*-$Al_{0.60}Ga_{0.40}N$ electron transport layer, a 300 nm undoped $Al_{0.70}Ga_{0.30}N$ absorption layer, 10 periods of AlN(8 nm)/$Al_{0.20}Ga_{0.80}N$(2 nm) MQW, and a 120 nm *p*-$Al_{0.50}Ga_{0.50}N$ hole transport layer are sequentially grown. Finally, the temperature is decreased to 1080°C, and a 50 nm heavily doped *p*-GaN contact layer is grown. For the reference device S_B, all growth and structure parameters are the same as that of S_A expect for the MQW. An *i*-$Al_{0.50}Ga_{0.50}N$ layer is grown to replace the MQW. Through adjusting the Al/Ga source ratio, the designed Al content can be realized. When the growth is finished, an *ex situ* thermal annealing at 900°C in N_2 is made to activate the Mg acceptors.

C. Device Fabrication

Standard semiconductor device fabrication processes are used to prepare the AlGaN SBUV detectors. First, a SiO_2 mask layer is deposited on the wafers by plasma-enhanced chemical vapor deposition, and the device pattern is transported to the mask layer by standard photolithography and reactive ion etching (RIE) processes. Then, the wafers are etched by an inductive coupling plasma etching system of about 600 nm to expose the *n*-$Al_{0.60}Ga_{0.40}N$ layer. After dissolving the residual SiO_2 mask by buffered oxide etching solution, the wafers are immersed in 10% NaOH solution at 80°C for 10 min to passivate the etching defects on the mesa sidewall. Next, the *n*-electrode pattern is transported to the wafer by photolithography and Ti 30 nm/Al 70 nm/Ni 50 nm/Au 150 nm electrode is deposited on the photolithograph-completed wafers by e-beam and thermal evaporation. After lift-off, the *n*-electrode is rapidly annealed at 600°C for 30 s in N_2 to form Ohmic contact. By the same processes, the *p*-electrode of Ni 50 nm/Au 150 nm is deposited on the mesa. After lift-off, the *p*-electrode is annealed at 550°C for 5 min in N_2 to form Ohmic contact. Finally, a SiO_2 passivation layer is deposited on the wafers to passivate the dangling bonds and thus to reduce leakage current. The SiO_2 layer on electrodes is then removed by RIE for performance test.

D. Characterizations

A high-resolution X-ray diffractometer (Brucker D8 DISCOVER) is adopted to estimate the Al content and crystal quality of the epilayers. A high-resolution scanning transmission electron microscope (HR-STEM) is employed to investigate the cross section of the devices, especially the MQW region. An optical microscope (OM, Nikon ECLIPSE LV15ONA) is used to observe the mesa and electrodes of the detectors. The current-voltage (*I-V*) curves are measured by the PDA FS-Pro 380 semiconductor analyzer. The spectral responses are measured by a DSR 100 system that is equipped with a xenon lamp, chopper, monochromator, Keithley 6487, SR830 lock-in amplifier, and standard Si detector. All response spectra are calibrated by the standard Si detector by considering the effective photosensitive area [40].

4. RESULTS AND DISCUSSION

The *I-V* curves of the two devices in dark and on illumination are calculated as shown in Fig. 3(a). The device S_A exhibits a significantly lower dark current than device S_B, demonstrating the MQW can effectively suppress the detector dark current. The decrease of dark current mainly results from the scattering effect of the band offset between the AlN barriers and AlGaN wells and the interface polarization charges. Besides, due to the strong QCSE, the generation-recombination current will also be suppressed. For the device S_A, within 40 V bias, the dark current slightly increases with the bias; for the device S_B, the dark current abruptly rises up at 10 V bias. It can be deduced that the MQW can promote the detector SNR in a large bias range as expected. On illumination, the photocurrent of device S_A is obviously greater than that of S_B, especially at low bias, which agrees well with our prediction. Accordingly, it demonstrates that device S_A has a higher response than S_B. The difference can be more intuitively reflected by the spectral responses, which are calculated by Eq. (3):

$$R(\lambda) = \frac{I_p(\lambda) - I_d(\lambda)}{P_{\text{in}}(\lambda)}, \tag{3}$$

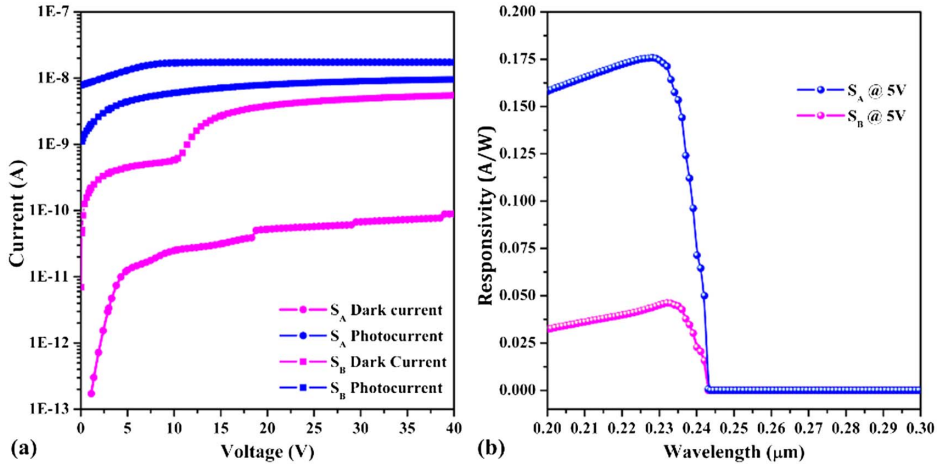

Fig. 3. (a) Simulated *I-V* curves in dark and on illumination for devices S_A and S_B. (b) Simulated spectral responses for devices S_A and S_B at 5 V bias.

where R is the responsivity, I_p and I_d are the photo and dark current, respectively and P_{in} is the incident light power. Figure 3(b) shows the response spectra of devices S_A and S_B at 5 V. Both devices possess the peak response at about 230 nm. However, device S_A has nearly four times higher peak response than S_B, directly confirming the positive effects of the MQW structure on the detector performance.

The energy band, current density, and carrier distributions are extracted to investigate the mechanism of the response gain. Figures 4(a) and 4(b) show the energy bands in the depletion regions for devices S_A and S_B at 5 V bias. The upper panels are in dark; the lower ones are on illumination. As is seen, the energy band bends upward along the [0001] direction for both devices, indicating the built-in electric field is also along the [0001] direction. However, there also exist differences between devices S_A and S_B. First, the energy band of the MQW in device S_A is serrated and the well layer energy band bends downward along the [0001] direction as predicted; the energy band for device S_B of the counterpart region for S_A is flat. Second, the energy band for the i-$Al_{0.70}Ga_{0.30}N$ region tilts more than that of the MQW in device S_A; it is just the opposite in device S_B. This means that the built-in electric field in the i-$Al_{0.70}Ga_{0.30}N$ absorption region is weaker than that in the MQW region for device S_A, and the case in S_B is exactly reverse. This phenomenon also originates from the polarization effect in AlGaN hetero-structure. In device S_A, the AlN layer on the i-$Al_{0.70}Ga_{0.30}N$ layer will induce positive polarization charges at the i-$Al_{0.70}Ga_{0.30}N$/AlN interface, creating an electric field along the [000–1] direction in the i-$Al_{0.70}Ga_{0.30}N$ layer and along the [0001] direction in the AlN barrier. In device S_B, the i-$Al_{0.50}Ga_{0.50}N$ layer on the i-$Al_{0.70}Ga_{0.30}N$ layer will induce negative polarization charges at the $Al_{0.70}Ga_{0.30}N$/$Al_{0.50}Ga_{0.50}N$ interface, creating an electric field along the [0001] direction in the i-$Al_{0.70}Ga_{0.30}N$ layer and along the [000–1] direction in the i-$Al_{0.50}Ga_{0.50}N$ layer. The differences will lead to two effects in device S_A: 1) the photogenerated electrons in the i-$Al_{0.70}Ga_{0.30}N$ layer are effectively prevented from diffusing to the MQWs and p-AlGaN layers; 2) the photogenerated holes are quickly swept into the MQW region and trapped by the MQW, resulting in net positive charges in the MQW region. In this case, electrons have to be drawn into the MQW from the cathode electrode to keep electrical neutrality. Because of the fast mobility, minimal intervalley electron scattering, strong built-in field, and prolonged lifetime, electrons will move fast and can travel multiple times through the devices, resulting in photoconductive gain.

Figures 4(c) and 4(d) show the electron and hole current profiles for devices S_A and S_B in dark and on illumination at 5 V bias, respectively. As the electrons are swept to the n-$Al_{0.60}Ga_{0.40}N$ region by the built-in electrical field, the current at the left boundary of the depletion region is mainly contributed by electrons. Similarly, the current at the right boundary of the depletion region is mainly contributed by holes. When observing the dark electron and hole currents at the left and right boundaries of the depletion region in Figs. 4(c) and 4(d), respectively, it is found that both dark electron and hole currents of device S_A are much lower than that of S_B, which may result from the trapping and scattering effects of the MQW as expected. However, on illumination, the hole current of device S_A is smaller than that of S_B, while the electron current is just the opposite. In Fig. 3(a), it is shown that the photocurrent of device S_A is higher than that of S_B. Therefore, it can be deduced that the photocurrent of device S_A is mainly contributed by electrons, while that of S_B is equally contributed by electrons and holes. This is evidence that the photoconductive gain has occurred in device S_A as predicted. Further, Figs. 4(e) and 4(f) display the electron and hole concentration distributions in devices S_A and S_B in dark and on illumination. As shown in Fig. 4(f), the hole concentration in the MQW region of device S_A increases significantly on illumination, while that of S_B hardly changes, indicating the hole trapping effect of the MQW. Besides, although the photogenerated

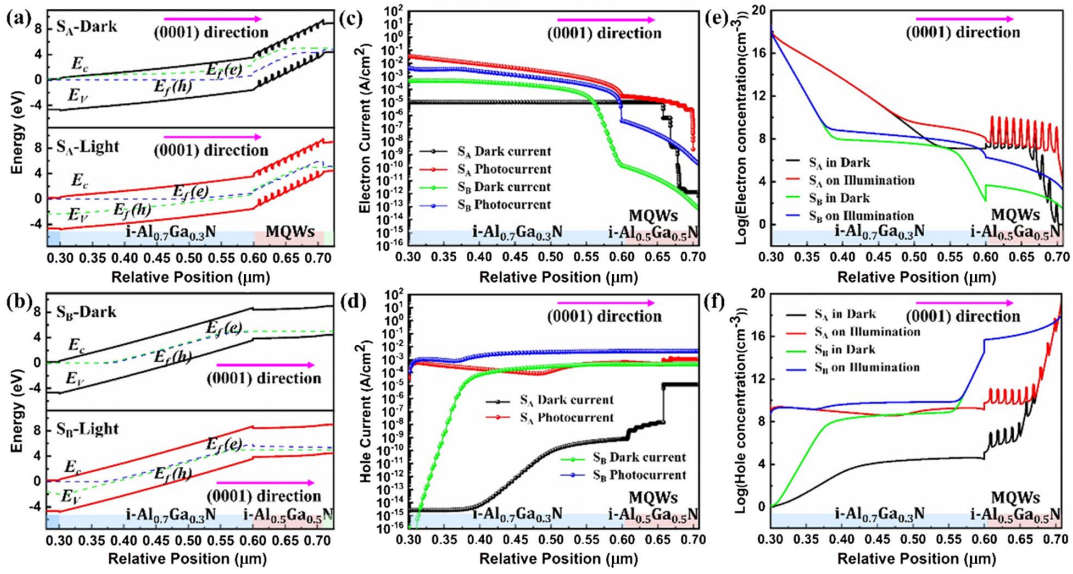

Fig. 4. Simulated energy bands for devices (a) S_A and (b) S_B, (c) electron and (d) hole current densities, (e) electron and (f) hole concentrations in dark and on illumination at 5 V bias, respectively.

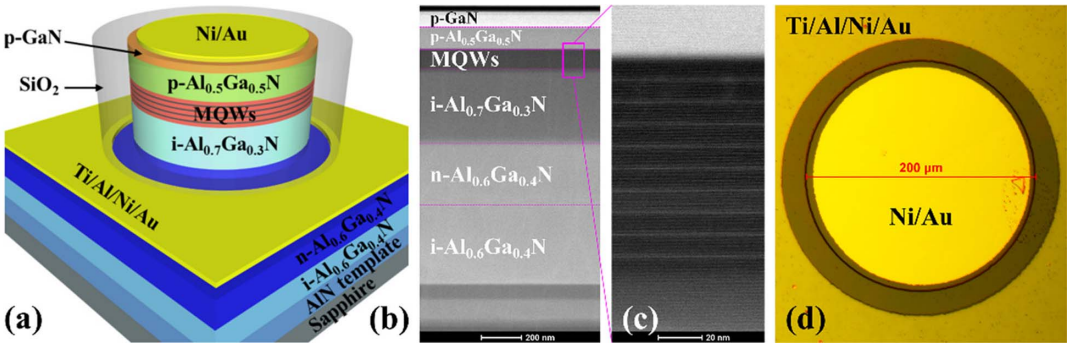

Fig. 5. (a) Schematic structure diagram of device S_A. (b) Cross-sectional STEM image of device S_A. (c) Enlarged STEM image for the MQW region in device S_A. (d) Plane-view OM image of the fabricated devices.

electrons are swept to the *n*-$Al_{0.60}Ga_{0.40}N$ side, the electron concentration in the MQW region is still improved, as shown in Fig. 4(e), implying the hole attracting effect and the prolonged carrier lifetime. Accordingly, it can be concluded that the MQW structure can introduce photoconductive gain into the vertical photodiode by prolonging the carrier lifetime via QCSE and making the electrons travel multiple times via electric field and electric neutrality effects.

Devices are experimentally fabricated to verify our conceptions. Figure 5(a) illustrates the schematic structure of device S_A. The reference device S_B has the same configuration expect for the MQW. Figure 5(b) displays the cross-sectional STEM image of the layer structure for device S_A. As is seen, the layers are grown as designed. To confirm the structure of the MQW, the HR-STEM image is measured as shown in Fig. 5(c). Clearly stacked structures are displayed. The narrow bright contrasts of about 2 nm are the wells, and the wide dark contrasts of about 8 nm are the barriers, respectively, demonstrating that the MQW region is grown as expected. Figure 5(d) shows the plane-view OM image for the fabricated devices. The diameter

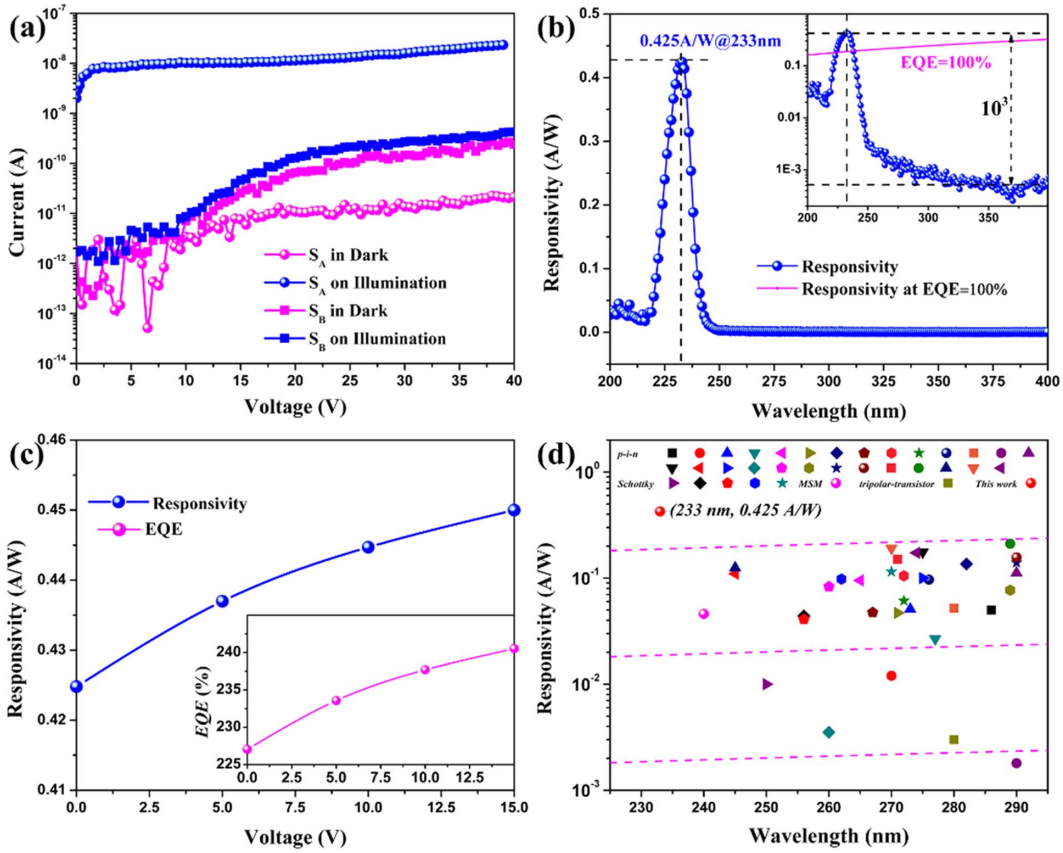

Fig. 6. (a) Photo and dark currents for devices S_A and S_B. (b) Spectral responses of device S_A at zero bias. Inset is the log-scale plot. (c) Bias-dependence of peak responsivity and EQE of device S_A. (d) Zero-bias peak responsivity and wavelength of device S_A and some reported AlGaN self-powered SBUV detectors [14,15,25,30,34,41–63].

is 200 μm, corresponding to an effective photosensitive area of about 31,416 μm^2, which is the used value in calibrating the responsivity. The devices are back-illuminated when working.

The *I-V* curves and spectral responses of devices S_A and S_B are measured to verify the detection performance. Figure 6(a) shows the *I-V* curves in dark and on illumination. The dark currents of both devices are small, which are at the magnitude of pA below 10 V bias. It may mainly come from the improved crystal quality by the AlN template, which can reduce the threading dislocation density and thus suppress the defect-assistant generation-recombination current. As the bias increases from 10 to 40 V, the dark current of device S_A just slightly becomes larger, while that of S_B obviously increases. It agrees well with the simulated results in Fig. 3(a). The carrier trapping and scattering effects by the MQW in device S_A shall be responsible for the suppression of dark current at relatively high biases. More importantly, when they are illuminated, the photocurrent of device S_A is much larger than that of S_B within all the measured biases, which also agrees well with the simulations, demonstrating the existence of photoconductive gain in device S_A. Certainly, the gain originates from the MQW because it can increase the carrier lifetime and induce unipolar carrier transport multiplication. It is worth noting that the photocurrent of device S_A at zero bias is also significantly promoted when it is compared with that of S_B, indicating that there exists photoconductive gain at even zero bias, which is important for improving the detector SNR. Comparing the photocurrent of devices S_A and S_B, it can be estimated that the gain can reach 10^3 in magnitude at zero bias.

Figure 6(b) shows the spectral response of device S_A at zero bias. The peak responsivity is 0.425 A/W at 233 nm, corresponding to an EQE of 226% calculated by Eq. (4):

$$\eta(\lambda) = \frac{1240 \cdot R(\lambda)}{\lambda}, \tag{4}$$

where η is the EQE, R is in the unit of A/W, and λ is the response wavelength in units of nm. The EQE much higher than 100% confirms the fact that there exists current gain in device S_A. Besides, the long-wavelength cutoff edge is shorter than 250 nm, ensuring the SBUV detection characteristic. Moreover, full-width at half-maximum of the response spectrum is just 13 nm, exhibiting excellent wavelength-selective characteristic. The inset in Fig. 6(b) shows the log-scale spectral response. As is seen, the responsivity ratio of peak wavelength to visible-blind ultraviolet band (365–400 nm) is about 10^3, indicating a good SNR of device S_A. It is worth noting that the sapphire substrate is single-polished. Therefore, we can speculate the responsivity can be much higher once the substrate is double-polished. Besides, we have ever attempted to measure the response spectrum of device S_B. Unfortunately, the photocurrent signal is below the equipment sensitivity, and we cannot obtain the response characteristic. Actually, the *I-V* curves have indicated the low performance of device S_B. This phenomenon further demonstrates the MQW structure has significant improvement on the detection performance. Figure 6(c) shows the bias dependence of the peak responsivity of device S_A; the inset is the corresponding EQE. The peak responsivity and EQE only slightly increase with the bias, which implies the carrier drift velocity and depletion region expansion are not the key factors limiting the performance. It further demonstrates that the carrier lifetime increase and the unipolar carrier transport multiplication caused by the MQW are primarily responsible for the performance improvement.

Figure 6(d) summarizes the zero-bias peak responsivity and its corresponding wavelength of this work and other reported self-powered AlGaN SBUV detectors. As is seen, although significant effort has been spent on improving the self-power performance over the past decades, the highest reported responsivity is just 0.211 A/W at 289 nm, corresponding to an EQE of 92%. The EQE below 100% indicates the current gain has not been realized in self-power work mode. Otherwise, because of the restriction by the crystal quality and *p*-doping of Al-rich nitrides, most of the reported AlGaN SBUV detectors work at wavelengths from 260 to 290 nm. Hence, even shorter wavelength detection capability can rarely be achieved. In our work, to our best knowledge, by introducing photoconductive gain into a vertical *p-i-n* photodiode via MQW structure, the highest zero-bias responsivity (0.425 A/W), shortest peak wavelength (233 nm), and highest EQE (226%) of self-powered AlGaN SBUV detector until now have been realized.

5. CONCLUSIONS

In summary, AlGaN SBUV detectors are investigated in this work. A photoconductive gain mechanism introduced into the vertical *p-i-n* photodiode is proposed to improve the performance of a self-powered AlGaN SBUV detector. Furthermore, the conception is realized through inserting MQW into the depletion region of an AlGaN *p-i-n* photodiode. Experimentally, the MQW-assisted photodiode exhibits a peak responsivity of about 0.425 A/W at 233 nm at zero bias, which is the highest responsivity as well as shortest peak wavelength AlGaN self-powered SBUV detector reported up to now. The corresponding zero-bias EQE of 226% demonstrates the internal photocurrent gain. When compared with the structure without MQW, the gain is estimated to be about 10^3 in magnitude. The MQW can bring about current gain mainly due to its strong hole confinement effect and the QCSE, resulting in a longer carrier lifetime and unipolar carrier transport, which are the key factors for generating photoconductive gain. The investigations have provided an alternative and effective approach to obtain high current gain in vertical structure AlGaN SBUV detectors at lower biases or even zero bias.

Funding. National Natural Science Foundation for Distinguished Young Scholars of China (61725403); National Natural Science Foundation of China (61827813, 61922078, 62004196); Youth Innovation Promotion Association of the Chinese Academy of Sciences (Y201945); Youth Talent Promotion Project of the Chinese Institute of Electronics (2020QNRC001); Key-Area Research and Development Program of Suzhou Institute of Nano-Tech and Nano-Bionics (20YZ10).

Disclosures. The authors declare no conflicts of interest.

REFERENCES

1. R. A. Yotter and D. M. Wilson, "A review of photodetectors for sensing light-emitting reporters in biological systems," IEEE Sens. J. **3**, 288–303 (2003).
2. Z. Y. Xu, H. P. Ding, B. M. Sadler, and G. Chen, "Analytical performance study of solar blind non-line-of-sight ultraviolet short-range communication links," Opt. Lett. **33**, 1860–1862 (2008).
3. W. J. Zhou, H. Li, X. Yi, J. Tu, and J. H. Yu, "A criterion for UV detection of AC corona inception in a rod-plane air gap," IEEE Trans. Dielectr. Electr. Insul. **18**, 232–237 (2011).
4. L. W. Sang, M. Y. Liao, Y. Koide, and M. Sumiya, "High-temperature ultraviolet detection based on InGaN Schottky photodiodes," Appl. Phys. Lett. **99**, 031115 (2011).
5. R. Z. Yuan and J. S. Ma, "Review of ultraviolet non-line-of-sight communication," China Commun. **13**, 63–75 (2016).
6. D. B. Li, K. Jiang, X. J. Sun, and C. L. Guo, "AlGaN photonics: recent advances in materials and ultraviolet devices," Adv. Opt. Photon. **10**, 43–110 (2018).
7. H. Ding, G. Chen, Z. Xu, and B. M. Sadler, "Channel modelling and performance of non-line-of-sight ultraviolet scattering communications," IET Commun. **6**, 514–524 (2012).
8. J. Y. Zheng, L. Wang, X. Z. Wu, Z. B. Hao, C. G. Sun, B. Xiong, Y. Luo, Y. J. Han, J. Wang, H. T. Li, J. Brault, S. Matta, M. A. Khalfioui, J. C. Yan, T. Wei, Y. Zhang, and J. X. Wang, "A PMT-like high gain avalanche photodiode based on GaN/AlN periodically stacked structure," Appl. Phys. Lett. **109**, 241105 (2016).
9. A. M. Armstrong, B. A. Klein, A. A. Allerman, A. G. Baca, M. H. Crawford, J. Podkaminer, C. R. Perez, M. P. Siegal, E. A. Douglas, V. M. Abate, and F. Leonard, "Visible- and solar-blind photodetectors using AlGaN high electron mobility transistors with a nanodot-based floating gate," Photon. Res. **7**, B24–B31 (2019).
10. K. Jiang, X. J. Sun, J. W. Ben, Y. P. Jia, H. N. Liu, Y. Wang, Y. Wu, C. H. Kai, and D. B. Li, "The defect evolution in homoepitaxial AlN layers grown by high-temperature metal-organic chemical vapor deposition," CrystEngComm **20**, 2720–2728 (2018).
11. K. Jiang, X. J. Sun, Z. M. Shi, H. Zang, J. W. Ben, H. X. Deng, and D. B. Li, "Quantum engineering of non-equilibrium efficient p-doping in ultra-wide band-gap nitrides," Light Sci. Appl. **10**, 69 (2021).
12. D. Walker, X. Zhang, P. Kung, A. Saxler, S. Javadpour, J. Xu, and M. Razeghi, "AlGaN ultraviolet photoconductors grown on sapphire," Appl. Phys. Lett. **68**, 2100–2101 (1996).
13. E. Monroy, F. Calle, and E. Munoz, "AlGaN metal semiconductor-metal photodiodes," Appl. Phys. Lett. **74**, 3401–3403 (1999).
14. H. Jiang and T. Egawa, "High quality AlGaN solar-blind Schottky photodiodes fabricated on AlN/sapphire template," Appl. Phys. Lett. **90**, 121121 (2007).
15. A. Kalra, S. Rathkanthiwar, R. Muralidharan, S. Raghavan, and D. N. Nath, "Polarization-graded AlGaN solar-blind p-i-n detector with 92% zero-bias external quantum efficiency," IEEE Photon. Technol. Lett. **31**, 1237–1240 (2019).
16. M. J. Hou, Z. X. Qin, C. G. He, L. S. Wei, F. J. Xu, X. Q. Wang, and B. Shen, "Study on AlGaN P-I-N-I-N solar-blind avalanche photodiodes with $Al_{0.45}Ga_{0.55}N$ multiplication layer," Electron. Mater. Lett. **11**, 1053–1058 (2015).
17. Q. Cai, K. X. Dong, Z. L. Xie, Y. Tang, J. J. Xue, and D. J. Chen, "Enhanced front-illuminated p-i-p-i-n GaN/AlGaN ultraviolet avalanche photodiodes," Mater. Sci. Semicond. Process. **96**, 24–29 (2019).
18. L. J. Sun, Z. S. Lv, Z. H. Zhang, X. J. Qiu, and H. Jiang, "High-performance AlGaN heterojunction phototransistor with dopant-free polarization-doped P-base," IEEE Electron Device Lett. **41**, 325–328 (2020).
19. M. Ishiguro, K. Ikeda, M. Mizuno, M. Iwaya, T. Takeuchi, S. Kamiyama, and I. Akasaki, "Control of the detection wavelength in AlGaN/GaN-based hetero-field-effect-transistor photosensors," Jpn. J. Appl. Phys. **52**, 08JF02 (2013).
20. J. A. Garrido, E. Monroy, I. Izpura, and E. Munoz, "Photoconductive gain modelling of GaN photodetectors," Semicond. Sci. Technol. **13**, 563–568 (1998).
21. B. W. Lim, Q. C. Chen, J. Y. Yang, and M. A. Khan, "High responsivity intrinsic photoconductors based on $Al_xGa_{1-x}N$," Appl. Phys. Lett. **68**, 3761–3762 (1996).
22. S. Butun, T. Tut, B. Butun, M. Gokkavas, H. B. Yu, and E. Ozbay, "Deep-ultraviolet $Al_{0.75}Ga_{0.25}N$ photodiodes with low cutoff wavelength," Appl. Phys. Lett. **88**, 123503 (2006).
23. I. S. Seo, I. H. Lee, Y. J. Park, and C. R. Lee, "Characteristics of UV photodetector fabricated by $Al_{0.3}Ga_{0.7}N$/GaN heterostructure," J. Cryst. Growth **252**, 51–57 (2003).
24. X. J. Sun, D. B. Li, Z. M. Li, H. Song, H. Jiang, Y. R. Chen, G. Q. Miao, and Z. W. Zhang, "High spectral response of self-driven GaN-based detectors by controlling the contact barrier height," Sci. Rep. **5**, 16819 (2015).
25. M. Brendel, M. Helbling, A. Knigge, F. Brunner, and M. Weyers, "Solar-blind AlGaN MSM photodetectors with 24% external quantum efficiency at 0 V," Electron. Lett. **51**, 1598–1600 (2015).
26. M. S. Shur and M. A. Khan, "GaN/AlGaN heterostructure devices: photodetectors and field-effect transistors," MRS Bull. **22**, 44–50 (1997).
27. T. Narita, A. Wakejima, and T. Egawa, "Ultraviolet photodetectors using transparent gate AlGaN/GaN high electron mobility transistor on silicon substrate," Jpn. J. Appl. Phys. **52**, 01AG06 (2013).
28. Z. G. Shao, X. F. Yang, H. F. You, D. J. Chen, H. Lu, R. Zhang, Y. D. Zheng, and K. X. Dong, "Ionization-enhanced AlGaN heterostructure avalanche photodiodes," IEEE Electron Device Lett. **38**, 485–488 (2017).
29. Q. Cai, W. K. Luo, R. Y. Yuan, H. F. You, Q. Li, M. Li, D. J. Chen, H. Lu, R. Zhang, and Y. D. Zheng, "Back-illuminated AlGaN heterostructure solar-blind avalanche with one-dimensional photonic crystal filter," Opt. Express **28**, 6027–6035 (2020).
30. W. Y. Han, Z. W. Zhang, Z. M. Li, Y. R. Chen, H. Song, G. Q. Miao, F. Fan, H. F. Chen, Z. Liu, and H. Jiang, "High performance back-illuminated MIS structure AlGaN solar-blind ultraviolet photodiodes," J. Mater. Sci. Mater. Electron. **29**, 9077–9082 (2018).
31. W. Yang, T. Nohava, S. Krishnankutty, R. Torreano, S. McPherson, and H. Marsh, "High gain GaN/AlGaN heterojunction phototransistor," Appl. Phys. Lett. **73**, 978–980 (1998).
32. M. L. Lee, J. K. Sheu, and Y.-R. Shu, "Ultraviolet bandpass $Al_{0.17}Ga_{0.83}N$/GaN heterojunction phototransistors with high optical gain and high rejection ratio," Appl. Phys. Lett. **92**, 053506 (2008).
33. S. J. Tang, L. X. Zhang, H. L. Wu, C. S. Liu, and H. Jiang, "Improved performance of ultraviolet AlGaN/GaN npn HPTs by a thin lightly-doped n-AlGaN insertion layer," AIP Adv. **9**, 125239 (2019).
34. L. X. Zhang, S. J. Tang, C. S. Liu, B. Li, H. L. Wu, H. L. Wang, Z. S. Wu, and H. Jiang, "Demonstration of solar-blind $Al_xGa_{1-x}N$-based heterojunction phototransistors," Appl. Phys. Lett. **107**, 233501 (2015).
35. O. Katz, A. Horn, G. Bahir, and J. Salzman, "Electron mobility in an AlGaN/GaN two-dimensional electron gas. I. Carrier concentration dependent mobility," IEEE Trans. Electron. Devices **50**, 2002–2008 (2003).
36. J. Schlegel, M. Brendel, M. Martens, A. Knigge, J. Rass, S. Einfeldt, F. Brunner, M. Weyers, and M. Kneissl, "Influence of carrier lifetime, transit time, and operation voltages on the photoresponse of visible-blind AlGaN metal-semiconductor-metal photodetectors," Jpn. J. Appl. Phys. **52**, 08JF01 (2013).
37. Z. H. Zhang, L. P. Li, Y. H. Zhang, F. J. Xu, Q. Shi, B. Shen, and W. G. Bi, "On the electric-field reservoir for III-nitride based deep ultraviolet light-emitting diodes," Opt. Express **25**, 16550–16559 (2017).
38. J. F. Muth, J. D. Brown, M. A. L. Johnson, Z. H. Yu, R. M. Kolbas, J. W. Cook, and J. F. Schetzina, "Absorption coefficient and refractive index of GaN, AlN and AlGaN alloys," Mater. Res. Soc. Internet J. Nitride Semicond. **4**, 502–507 (1999).
39. D. Brunner, H. Angerer, E. Bustarret, F. Freudenberg, R. Hopler, R. Dimitrov, O. Ambacher, and M. Stutzmann, "Optical constants of epitaxial AlGaN films and their temperature dependence," J. Appl. Phys. **82**, 5090–5096 (1997).
40. K. Jiang, X. J. Sun, Z. H. Zhang, J. W. Ben, J. M. Che, Z. M. Shi, Y. P. Jia, Y. Chen, S. L. Zhang, W. Lv, and D. B. Li, "Polarization-enhanced AlGaN solar-blind ultraviolet detectors," Photon. Res. **8**, 1243–1252 (2020).

41. G. Parish, S. Keller, P. Kozodoy, J. P. Ibbetson, H. Marchand, and P. T. Fini, "Low dark current p-i-n (Al,Ga)N-based solar-blind UV detectors on laterally epitaxially overgrown GaN," in *Conference on Optoelectronic & Microelectronic Materials Devices* (1998), pp. 175–178.
42. C. Pernot, A. Hirano, M. Iwaya, T. Detchprohm, H. Amano, and I. Akasaki, "Solar-blind UV photodetectors based on GaN/AlGaN p-i-n photodiodes," Jpn. J. Appl. Phys. **39**, L387–L389 (2000).
43. J. D. Brown, J. Z. Li, P. Srinivasan, J. Matthews, and J. F. Schetzina, "Solar-blind AlGaN heterostructure photodiodes," MRS Internet J. Nitride Semicond. Res. **5**, 35–37 (2000).
44. D. J. H. Lambert, M. M. Wong, U. Chowdhury, C. Collins, T. Li, H. K. Kwon, B. S. Shelton, T. G. Zhu, J. C. Campbell, and R. D. Dupuis, "Back illuminated AlGaN solar-blind photodetectors," Appl. Phys. Lett. **77**, 1900–1902 (2000).
45. J. P. Long, S. Varadaraajan, J. Matthews, and J. F. Schetzina, "UV detectors and focal plane array imagers based on AlGaN p-i-n photodiodes," Opto-Electron Rev. **10**, 251–260 (2002).
46. N. Biyikli, I. Kimukin, O. Aytur, and E. Ozbay, "Solar-blind AlGaN-based p-i-n photodiodes with low dark current and high detectivity," IEEE Photon. Technol. Lett. **16**, 1718–1720 (2004).
47. R. McClintock, A. Yasan, K. Mayes, D. Shiell, S. R. Darvish, P. Kung, and M. Razeghi, "High quantum efficiency AlGaN solar-blind p-i-n photodiodes," Appl. Phys. Lett. **84**, 1248–1250 (2004).
48. E. Ozbay, T. Tut, and N. Biyikli, "High-performance solar-blind AlGaN photodetectors," Proc. SPIE **5732**, 375–388 (2005).
49. M. B. Reine, A. Hairston, P. Lamarre, K. K. Wong, S. P. Tobin, A. K. Sood, C. Cooke, M. Pophristic, S. Guo, B. Peres, R. Singh, C. R. Eddy, Jr., U. Chowdhury, M. M. Wong, R. D. Dupuis, T. Li, and S. P. DenBaars, "Solar-blind AlGaN 256×256 p-i-n detectors and focal plane arrays," Proc. SPIE **6119**, 611901 (2006).
50. T. Tut, T. Yelboga, E. Ulker, and E. Ozbay, "Solar-blind AlGaN-based p-i-n photodetectors with high breakdown voltage and detectivity," Appl. Phys. Lett. **92**, 103502 (2008).
51. D. G. Zhao, S. Zhang, D. S. Jiang, J. J. Zhu, Z. S. Liu, H. Wang, S. M. Zhang, B. S. Zhang, and H. Yang, "A study on the spectral response of back-illuminated p-i-n AlGaN heterojunction ultraviolet photodetector," J. Appl. Phys. **110**, 053701 (2011).
52. X. J. Sun, D. B. Li, Y. R. Chen, H. Song, H. Jiang, Z. M. Li, G. Q. Miao, and Z. W. Zhang, "*In situ* observation of two-step growth of AlN on sapphire using high-temperature metal-organic chemical vapour deposition," CrystEngComm **15**, 6066–6073 (2013).
53. E. Cicek, R. McClintock, C. Y. Cho, B. Rahnema, and M. Razeghi, "$Al_xGa_{1-x}N$-based back-illuminated solar-blind photodetectors with external quantum efficiency of 89%," Appl. Phys. Lett. **103**, 191108 (2013).
54. B. Albrecht, S. Kopta, O. John, M. Rutters, M. Kunzer, R. Driad, N. Marenco, K. Kohler, M. Walther, and O. Ambacher, "Improved AlGaN p-i-n photodetectors for monitoring of ultraviolet radiation," IEEE J. Sel. Top. Quantum Electron. **20**, 166–172 (2014).
55. X. J. Li, D. G. Zhao, D. S. Jiang, Z. S. Liu, P. Chen, L. C. Le, J. Yang, and X. G. He, "Performance comparison of front- and back-illuminated modes of the AlGaN-based p-i-n solar-blind ultraviolet photodetectors," J. Vac. Sci. Technol. B **32**, 031204 (2014).
56. Y. R. Chen, Z. W. Zhang, Z. M. Li, H. Jiang, G. Q. Miao, and H. Song, "The influence of n-AlGaN inserted layer on the performance of back-illuminated AlGaN-based p-i-n ultraviolet photodetectors," Phys. Status Solidi A **215**, 1700358 (2017).
57. Y. R. Chen, Z. W. Zhang, H. Jiang, Z. M. Li, G. Q. Miao, and H. Song, "The optimized growth of AlN templates for back-illuminated AlGaN-based solar-blind ultraviolet photodetectors by MOCVD," J. Mater. Chem. C **6**, 4936–4942 (2018).
58. T. T. T. Pham, J. H. Choi, C. H. Cho, and H. Y. Cha, "Filter-free AlGaN photodiode with high quantum efficiency for partial discharge detection," J. Semicond. Technol. Sci. **20**, 141–144 (2020).
59. Z. K. Cao, D. G. Zhao, F. Liang, and Z. S. Liu, "Fabrication of high quantum efficiency p-i-n AlGaN detector and optimization of p-layer and i-layer thickness," Mater. Res. Express **7**, 115902 (2020).
60. Y. R. Chen, Z. W. Zhang, G. Q. Miao, H. Jiang, Z. M. Li, and H. Song, "Epitaxial growth of polarization-graded AlGaN-based solar-blind ultraviolet photodetectors on pre-grown AlN templates," Mater. Lett. **281**, 128638 (2020).
61. N. Biyikli, O. Aytur, I. Kimukin, T. Tut, and E. Ozbay, "Solar-blind AlGaN-based Schottky photodiodes with low noise and high detectivity," Appl. Phys. Lett. **81**, 3272–3274 (2002).
62. H. Jiang, T. Egawa, and H. Ishikawa, "AlGaN solar-blind Schottky photodiodes fabricated on 4H-SiC," IEEE Photon. Technol. Lett. **18**, 1353–1355 (2006).
63. Z. Q. Huang, J. F. Li, W. L. Zhang, and H. Jiang, "AlGaN solar-blind avalanche photodiodes with enhanced multiplication gain using back-illuminated structure," Appl. Phys. Express **6**, 054101 (2013).